Dual regulation of the native ClC-K2 chloride channel in the distal nephron by voltage and pH

Laurent Pinelli, Antoine Nissant, Aurélie Edwards, Stéphane Lourdel, Jacques Teulon, Marc Paulais

Published August 29, 2016

Dual regulation of the native ClC-K2 chloride channel in the distal nephron by voltage and pH

Laurent Pinelli,[1,2,3,4]* Antoine Nissant,[1,2,3,4]* Aurélie Edwards,[1,2,3,4] Stéphane Lourdel,[1,2,3,4] Jacques Teulon,[1,2,3,4] and Marc Paulais[1,2,3,4]

[1]Sorbonne Universités, Université Pierre-et-Marie-Curie Paris 06, [2]Institut National de la Santé et de la Recherche Médicale, and [3]Université Paris Descartes, Sorbonne Paris Cité, UMR_S 1138, Centre de Recherche des Cordeliers, F-75006 Paris, France
[4]Centre National de la Recherche Scientifique ERL 8228, Centre de Recherche des Cordeliers, F-75006 Paris, France

ClC-K2, a member of the ClC family of Cl^- channels and transporters, forms the major basolateral Cl^- conductance in distal nephron epithelial cells and therefore plays a central role in renal Cl^- absorption. However, its regulation remains largely unknown because of the fact that recombinant ClC-K2 has not yet been studied at the single-channel level. In the present study, we investigate the effects of voltage, pH, Cl^-, and Ca^{2+} on native ClC-K2 in the basolateral membrane of intercalated cells from the mouse connecting tubule. The ∼10-pS channel shows a steep voltage dependence such that channel activity increases with membrane depolarization. Intracellular pH (pH_i) and extracellular pH (pH_o) differentially modulate the voltage dependence curve: alkaline pH_i flattens the curve by causing an increase in activity at negative voltages, whereas alkaline pH_o shifts the curve toward negative voltages. In addition, pH_i, pH_o, and extracellular Ca^{2+} strongly increase activity, mainly because of an increase in the number of active channels with a comparatively minor effect on channel open probability. Furthermore, voltage alters both the number of active channels and their open probability, whereas intracellular Cl^- has little influence. We propose that changes in the number of active channels correspond to them entering or leaving an inactivated state, whereas modulation of open probability corresponds to common gating by these channels. We suggest that pH, through the combined effects of pH_i and pH_o on ClC-K2, might be a key regulator of NaCl absorption and Cl^-/HCO_3^- exchange in type B intercalated cells.

INTRODUCTION

It is widely acknowledged that ClC-Kb in humans (ClC-K2 in rodents), in association with the regulatory subunit barttin, is the main basolateral chloride channel in the distal nephron and is therefore of prime importance in NaCl absorption, body salt homeostasis, and possibly long-term blood pressure regulation (Jentsch, 2008; Fahlke and Fischer, 2010; Staruschenko, 2012; Eladari et al., 2014; Andrini et al., 2015; Sepúlveda et al., 2015). Bartter's syndrome type III, a rare salt- and potassium-losing tubulopathy that targets the thick ascending limb (TAL) and the distal convoluted tubule (DCT), is caused by loss-of-function *CLCKNB* mutations leading to impairment of NaCl balance and hypokalemic metabolic alkalosis (Krämer et al., 2008; Stölting et al., 2014; Andrini et al., 2015). The recent description of a severe Bartter's syndrome in *Clcnk2*$^{-/-}$ mice ascertained that ClC-K2 plays a similar role in the mouse (Hennings et al., 2016).

Although the ClC family of chloride channels and transporters to which the ClC-K channels belong has been extensively studied from a biophysical standpoint (Pusch et al., 1999; Pusch, 2004; Chen, 2005), this is not the case for ClC-K channels because their expression in heterologous systems, especially that of ClC-K2 (Kieferle et al., 1994; Waldegger and Jentsch, 2000; Fahlke and Fischer, 2010), remains difficult to achieve (Estévez et al., 2001; Waldegger et al., 2002; Gradogna et al., 2010). ClC-K channels display a feature unique among ClC isoforms in that their activity increases with extracellular Ca^{2+} and pH (Estévez et al., 2001; Waldegger et al., 2002; Gradogna et al., 2010, 2012; Andrini et al., 2014). In addition, ClC-K channels share the unique double-barreled architecture of ClC channels with two independent ion conduction pores. However, they lack the characteristic glutamate residue involved in the protopore gate mechanism of ClC channels, and their gating is probably dominated by the common gate (Pusch, 2004; Jentsch, 2008; Stölting et al., 2014).

It has not been possible yet to study recombinant ClC-K2 or ClC-Kb at the single-channel level (Fahlke and Fischer, 2010; Stölting et al., 2014). Patch clamp studies on basolateral membranes of mouse renal tubules identified an ∼10-pS Cl^- channel in the DCT, in the intercalated cells of the connecting tubule (CNT) and cortical collecting duct (CCD; Lourdel et al., 2003;

*L. Pinelli and A. Nissant contributed equally to this paper.
Correspondence to Jacques Teulon: jacques.teulon@upmc.fr
A. Nissant's present address is Centre National de la Recherche Scientifique UMR3571, Institut Pasteur, 75015 Paris, France.

Abbreviations used: CCD, cortical collecting duct; CNT, connecting tubule; DCT, distal convoluted tubule; TAL, thick ascending limb.

The Rockefeller University Press $30.00
J. Gen. Physiol. 2016 Vol. 148 No. 3 213–226
www.jgp.org/cgi/doi/10.1085/jgp.201611623

Supplemental Material can be found at:
http://jgp.rupress.org/content/suppl/2016/08/18/jgp.201611623.DC1.html

Published August 29, 2016

Nissant et al., 2004, 2006; Teulon et al., 2005) and, more recently, in the TAL (Hennings et al., 2016). The channel was highly sensitive to intracellular pH (pH_i) and inhibited by PKC but insensitive to PKA (Lourdel et al., 2003). It required ATP for maintaining its activity in the inside-out configuration and was present at high density in membrane patches (Lourdel et al., 2003; Nissant et al., 2004, 2006). We considered the ∼10-pS Cl^- channel as a likely ClC-K2 candidate because it displayed an anionic selectivity sequence and sensitivity to external Ca^{2+} and pH similar to that of ClC-Kb. In fact, recent patch-clamp analysis revealed the complete absence of the ∼10 pS Cl^- channel in *Clcnk2*$^{-/-}$ mice, giving a direct proof of its molecular identity (Hennings et al., 2016).

The objective of the present study was to examine in detail how classical modulators of ClC and ClC-K channels (Miller and White, 1980; Rychkov et al., 1996; Pusch et al., 1999; Chen and Chen, 2001; Fahlke, 2001), i.e., membrane voltage, pH_i and extracellular pH (pH_o), extracellular Ca^{2+}, and intracellular Cl^- might modulate native ClC-K2 activity. Our results first show that the native ClC-K2 is voltage dependent, a property not yet recognized in recombinant ClC-Kb/K2 channels, and activates upon membrane depolarization via an increase in the number of active channels and to a lesser extent in the open probability. Dependence on voltage is differentially modulated by pH_i and pH_o in such a way that channel activity synergistically increases with pH around resting membrane voltage. Second, we report that an elevation in pH_i, as well as in external calcium and pH, increases ClC-K2 activity mainly via the modulation of the number of active channels. Therefore, we propose that powerful pH-dependent processes modulate the main pathway for basolateral Cl^- exit from cells along the distal nephron, and hence renal NaCl transport, by controlling the number of active channels.

MATERIALS AND METHODS

Isolation of renal tubules

The experiments were conducted according to the standards of the Veterinary Department of the French Ministry of Agriculture, and procedures were approved by the Ethics Committee at the Pierre and Marie Curie University (agreement Ce5/2011/040). Tissue preparation was as previously described (Nissant et al., 2006). In brief, 15–20-g male mice (Charles River) were killed by cervical dislocation, and the left kidney was perfused with Leibovitz's L-15 medium (Sigma-Aldrich) supplemented with 300 U/ml Worthington CLS-2 collagenase (Coger) before removal. Small pieces of cortex were incubated at 37°C for 30–60 min in the collagenase-containing medium, rinsed, and kept at 4°C until use.

Solutions and chemicals

Patch pipettes were filled with a solution containing (mM) 145 NMDG-Cl, 1 $MgCl_2$, and 10 HEPES and adjusted to pH 7.0–7.8 using NMDG. For adjustment to pH 6.6, 10 mM Mes was substituted for HEPES. Pipette solution calcium content was set by adding appropriate amounts of $CaCl_2$. The tubules were initially bathed in physiological saline containing (mM) 140 NaCl, 5 KCl, 1 $CaCl_2$, 1 $MgCl_2$, 10 glucose, and 10 HEPES and adjusted to pH 7.4 with NaOH. NMDG-Cl was substituted for NaCl in the Na^+-free solution used for determination of the number of channels in cell-attached patches (see below in Data analysis section). Membrane patches were excised into a solution containing (mM) 145 NMDG-Cl, 1 $MgCl_2$, and 10 glucose and buffered with either 10 HEPES or 10 Trizma base for adjustment to pH 7.0–7.8 or pH 8.2, respectively, using NMDG. When necessary, internal Cl^- concentrations ranging from 7 to 147 mM were obtained by using the appropriate amount of NMDG-Cl and by adjusting osmolarity with sucrose. In the inside-out configuration, 2 mM EGTA (no Ca^{2+} added) and 0.5–1 mM Mg-ATP (Sigma-Aldrich) were added to the perfusion solutions to partially prevent rundown (Lourdel et al., 2003; Nissant et al., 2006). Usually, an important fraction of the channels in the patch membrane underwent rapid rundown after excision from the cell, but the remaining channels could be recorded for long periods of time (5–20 min) provided that ATP was present in the internal solution.

Current recordings

Patch pipettes were pulled from Harvard Apparatus GC150T borosilicate glass (Phymep) by a P-97 puller (Sutter Instrument), coated with SYLGARD, and heat polished. Single-channel currents were amplified with a List LM-EPC7 or a Bio-logic RK 400 patch-clamp amplifier, filtered at 300 or 500 Hz by a LPBF-48DG 8-pole Bessel filter (NPI Electronic), and digitized at a sampling rate of 1–2 kHz using DIGIDATA 1322A or 1440A analogue to digital converters and P-CLAMP software (Axon Instruments) for online monitoring and recording. All experiments were performed at room temperature (22–27°C).

Data analysis

Stretches of data of 30-s to 1-min duration were analyzed for each condition. Channel activity on a patch was determined by the time-averaged Cl^- current passing through the patch ($\langle I \rangle$), taking the closed channel current level as reference, divided by the unitary current amplitude *i*. This method assumes that all the chloride channels present in the membrane patch behave in the same homogenous way. The high number of channels per patch and the slow channel kinetics with open and closed times in the second range (Lour-

Published August 29, 2016

del et al., 2003) often precluded the determination of the closed current level by visual inspection of the recording, and inhibition of channel activity was therefore required. In cell-attached patches, this was obtained by the lowering of pH_i under tubule superfusion with a Na^+-free solution supplemented with either 0.25 mM *N*-ethylmaleimide (Sigma-Aldrich; Nissant et al., 2006) or 20 mM sodium acetate (Lourdel et al., 2003). A long delay of 1–5 min in these conditions was usually needed to reach a plateau for the minimum current level. In the inside-out configuration, the closed level was determined under low pH bath solution or at the end of recording when channel activity had sufficiently run down. Routinely, our experimental sequences lasted 20–30 s.

In this study, we suggest that variations in the number of active channels involve very slow gating processes (>20 s), whereas variations in open probability (P_o) concern more rapid opening/closing events (still in the second range). In other words, modulation of the number of active channels might be caused by channels entering or leaving an inactivated state, whereas modulation of the open probability might stem from more rapid oscillations between open and closed states. Accordingly, we defined N′ as the number of active channels in a given experimental condition as $N' = N * P_{o\ slow}$, where N is the absolute number of channels on the patch (an unknown parameter) and $P_{o\ slow}$ represents the open probability caused by kinetic processes >20–30 s (also an unknown parameter). Experimentally, N′ represents the highest number of simultaneously open channels during one experimental sequence. N′ was determined by either visual inspection of patches containing only few levels of currents or by measuring the peak current amplitude, subtracting the closed current level, and dividing by the single channel current amplitude *i*. Thus, in the following, we use the equation $I/i = N' * P_o$ to calculate P_o.

We checked the accuracy of this evaluation by independently estimating P_o and N′ using stationary noise analysis (Gray, 1994). Here, the determination of the variance of the current (σ^2) in each stretch of data enabled the calculation of P_o and N′ according to the equations $1 - P_o = \sigma^2/(<I> * i)$ and $N' = <I>/(i * P_o)$. The relative difference in N′ deduced from the peak (N'_{peak}) and variance ($N'_{\sigma 2}$) methods $((N'_{peak} - N'_{\sigma 2})/N'_{peak})$ was then plotted versus $1 - P_o$ (Fig. S1). Only recordings yielding $\Delta N'/N'$ values within a 95% agreement interval were included in this analysis (Bland and Altman, 1999). As emphasized by several authors, the number of channels along a stretch of recording can be underestimated; in the meantime, it has the advantage of being a direct measurement (Pácha et al., 1993; Colquhoun and Hawkes, 1995).

$N'P_o/V$ data points were fitted by Boltzmann's function:

$$Y = \frac{Y\min - Y\max}{1 + e^{(V - V_{1/2})/K}} + Y\min,$$

where V is a given membrane potential difference, $V_{1/2}$ is the potential difference yielding a half-maximal response, Ymin and Ymax are the minimum and maximum $N'P_o$ values, respectively, and K is the logarithmic sensitivity indicating an e-fold increase in membrane potential difference. OriginLab Corporation ORIGIN software (Ritme Informatique) was used to fit the data points to equations.

P-CLAMP–generated amplitude histograms were fitted by a multiple peak Gaussian function using ORIGIN software, and the area of each component (k) relative to the total area of the *n* components was used to calculate its open probability, $P_{(k)}$. $P_{(k)}$ values were then compared with the distribution of k simultaneously open independent channels predicted by a binomial distribution, according to the equation

$$P_{(k)} = \frac{n!}{k!(n-k)!} P_o^k (1 - P_o)^{n-k}.$$

Mathematical model of type B intercalated cells

The mathematical model of the type B intercalated cell is based on steady-state conservation equations for mass and charge, following the approach of Weinstein (2001). These equations yield the intracellular volume, electric potential, and the concentrations of 12 solutes as a function of external conditions. Our CCD model differs from that of Weinstein (2001) in that it accounts for the NaCl transport pathway in type B intercalated cells described by Eladari and colleagues (Leviel et al., 2010; Chambrey et al., 2013). Thus, in contrast with the Weinstein (2001) model, our model considers the presence of apical Na^+-dependent Cl^-/HCO_3^- exchangers (NDBCE), and it assumes that basolateral AE4 transporters, the transport properties of which remain controversial, operate as Na^+-HCO_3^- cotransporters (with a Na^+/HCO_3^- stoichiometry of 1:3 as required for a sodium extruder) and that the basolateral permeability to HCO_3^- is zero. The simulations performed in this study correspond to asymmetrical conditions, that is, with 144 mM Na^+, 4 mM K^+, and 118 mM Cl^- in the peritubular solution, pH 7.4, and 75 mM Na^+, 15 mM K^+, and 75 mM Cl^- in the lumen, pH 7.04.

Statistics

Results are given as means ± SEM for the indicated number of measurements (*n*). Statistical significance of difference between means of groups was evaluated by either Student's *t* test or by one-way ANOVA, when appropriate, using Systat SIGMASTAT software (Ritme Informatique). $P < 0.05$ was considered significant.

Published August 29, 2016

Online supplemental material

Fig. S1 compares the results from peak current and stationary noise analysis methods for the estimation of the number of active ClC-K2 channels on patches. Fig. S2 illustrates ClC-K2 channel conductive properties and voltage dependence in the cell-attached configuration. Fig. S3 shows ClC-K2 sensitivity to intracellular chloride. Fig. S4 depicts the variations in N′ and P_o induced by changes in pH_o and $Ca^{2+}{}_o$. Table S1 summarizes single-channel conductive properties under various pH_i, pH_o, and $[Ca^{2+}]_o$ conditions.

RESULTS

We previously showed that a small-conductance Cl^- channel was densely present in the basolateral membranes of the TAL, DCT, and the intercalated cells of the CNT/CCD (Lourdel et al., 2003; Nissant et al., 2004, 2006). As anticipated (Lourdel et al., 2003; Teulon et al., 2005), recent work has demonstrated that this channel is formed by ClC-K2 (Hennings et al., 2016). In the present study on CNT intercalated cells, the channel displayed a unitary conductance of ∼10 pS (Fig. 1 A and Table S1), in agreement with previous results (Nissant et al., 2006). We observed 1–14 channels in the inside-out configuration at pH 7.4 (Fig. 1 B), but the number of channels can be considerably higher at more alkaline pH (see below Fig. 3). Even and odd numbers of equally spaced current (10-pS conductance) levels were observed (Fig. 1 B). If the observed ClC-K2 currents levels reflected the openings of independently gated protopores, an even number of conductance states should have been observed (Fischer et al., 2010; Stölting et al., 2014). A typical current trace of native ClC-K2 in a cell-excised inside-out patch from CNT intercalated cells bathed in symmetrical NMDG-Cl^- solutions is shown in Fig. 1 C. Current levels were equidistant (Fig. 1 D) and followed a binomial distribution (Fig. 1 E), again suggesting that protopore gating was not detected in this channel. Half-openings probably representing openings/closings of the protopore (Lourdel et al., 2003) could be detected from time to time but were generally brief, except at the end of long recordings when channels were inactivating (Fig. 1 F). Altogether, the 10-pS conductance most probably reflects oscillations of the ClC-K2 dimeric structure, indicating that channel gating is dominated by the common gate.

Native ClC-K2 channel activity is highly dependent on voltage

One objective of this study was to investigate whether native ClC-K2 is sensitive to voltage. We first addressed this issue in inside-out patches by systematically quantifying channel activity at various membrane voltages and observed that patch currents dramatically increased at

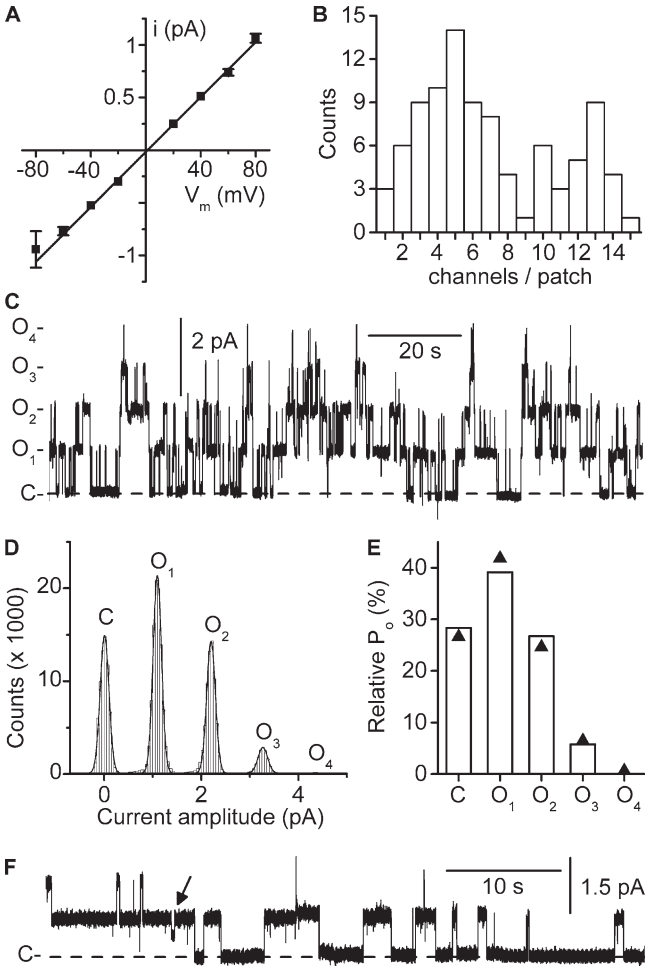

Figure 1. **Conductive properties of the native ClC-K2 channel.** Experiments were performed on cell-excised inside-out membrane patches under symmetrical NMDG-Cl conditions. Pipette solution contained 5 mM Ca^{2+}, and pipette and bath pH were set to 7.4. (A) Mean i/V_m relationship. Each point is the mean of 12 determinations, and SEM is shown as error bars when larger than symbols. The straight line is a linear fit of mean data points yielding a conductance of 13 ± 0.2 pS and a reversal potential of 1.7 ± 0.7 mV (R^2 = 0.998). (B) Channel density distribution. The maximum number of active channels per patch was determined by peak current measurement, at V_m 80 mV (92 patches). Note the even and odd numbers of channels/patch. (C) Continuous channel recording at V_m 80 mV. The dashed line indicates the closed channel current level (C-), and O_1- to O_4- indicate the current levels corresponding to the opening of one to four channels. (D) Point-amplitude histogram of the recording shown in C (0.05 pA bins). For clarity, the closed channel current level was subtracted. The continuous line is a nonlinear least square 5-term Gaussian fit of amplitude distribution data yielding peaks of 0.009 ± 0.001 pA (C), 1.09 ± 0.001 pA (O_1), 2.2 ± 0.001 pA (O_2), 3.3 ± 0.006 pA (O_3), and 4.4 pA (O_4; R^2 = 0.997). (E) Probabilities of the channel current states in the recording shown in C. The measured state probabilities (bars) are shown together with the probability values predicted by a binomial distribution (▲; see Materials and methods) with k = 5 current levels including baseline and P_o = 0.282. (F) Continuous recording from a patch with only two apparent active channels. The dashed line indicates the closed channel current level (C-). Note the infrequent short-lived subconductance state (arrow).

Published August 29, 2016

positive membrane voltages (Fig. 2). For instance, for the traces shown in Fig. 2 A, $N'P_o$ increased from 2.5 at V_m −80 mV to 7.9 at V_m 80 mV. The data from 10 patches confirm that channel activity is highly dependent on membrane voltage (Fig. 2 B); the Boltzmann fit of mean $N'P_o$ data points yielded K and $V_{1/2}$ values of 11 ± 7.3 mV and 44 ± 3.5 mV, respectively. Note that $N'P_o$ stays relatively low over the range of physiological membrane voltages encountered in epithelial cells (between −70 and −30 mV, depending on cell type).

The properties of the channel in the cell-attached configuration are illustrated in Fig. S2. In these conditions, channel conductance was 10.4 ± 0.2 pS (n = 12, Fig. S2 B). The examination of traces in Fig. S2 A shows that the channel voltage dependence is preserved in situ, $N'P_o$ increasing in this example from 4.1 at a clamp potential (V_c) of −80 mV to 13.6 at V_c of 80 mV. The results from nine cell-attached patches are quantified in Fig. S2 C.

The variations in voltage occurring in CNT cells are very likely too limited to produce by themselves noticeable alterations in channel activity. Nevertheless, such a regulation could be of importance in the physiological control of channel activity, if any regulatory factor had the power of altering the shape of the voltage dependence curve. In the following measurements, we therefore examined whether pH_i, pH_o, and calcium concentration ($[Ca^{2+}]_o$), which are known regulators of the native ClC-K2 channel (Lourdel et al., 2003; Nissant et al., 2006), as well as intracellular chloride concentration ($[Cl^-]_i$), which influences the activity of ClC-0 and ClC-2 (Pusch et al., 1999; Niemeyer et al., 2003; Yusef et al., 2006), are able to alter ClC-K2 voltage dependence.

Channel activity is relatively independent of $[Cl^-]_i$

To date, the possibility that $[Cl^-]_i$ might regulate recombinant and native ClC-K2 channels and potentially contribute to the cross-talk between apical entry and basolateral exit of chloride in renal cells has not been explored. Thus, we measured ClC-K2 activity in cell-excised inside-out patches clamped at either V_m 80 or V_m −80 mV, while decreasing $[Cl^-]_i$ from 147 to 7 mM. As illustrated in Fig. S3, $N'P_o$ did not change much over the 147–14.5 mM $[Cl^-]_i$ range at both potentials. Further lowering $[Cl^-]_i$ down to 7 mM, a value well below the resting $[Cl^-]_i$ in the renal cells (Greger et al., 1983; Beck et al., 1988; Weinstein, 2005), decreased $N'P_o$ to ∼65% and ∼32% of the $N'P_o$ at 147 mM at V_m −80 mV (n = 3) and V_m 80 mV (n = 3), respectively (P = 0.05 for each potential, paired Student's t test). In sum, variations in $[Cl^-]_i$ within the physiological range have a limited effect on ClC-K2 activity and voltage dependence.

Alkaline pH_i flattens the voltage dependence curve by increasing $N'P_o$ at negative membrane voltage

We have previously demonstrated that the native ClC-K2 is sensitive to pH_i (Lourdel et al., 2003; Nissant et al., 2006). Here, we attempted to establish a dose–response curve over an extended pH_i range (Fig. 3). The $N'P_o$ values were very low at pH_i 6.6 (0.003 ± 0.003, n = 4) and 7.0 (0.15 ± 0.11, n = 4) and increased substantially over the 7.0–7.8 range, and even more steeply when pH_i was raised from 7.8 to 8.2. Although we cannot ascertain that the maximal response was reached at pH_i 8.2 because patch instability precluded a more complete analysis at higher pH_i values, our results strongly indicate that pKa might be well above physiologically relevant pH_i values.

We examined whether pH_i alters the ClC-K2 voltage dependence by comparing activities in the same patches at negative and positive membrane voltages while pH_i was varied over the 7.0–7.8 range. A rise in pH_i from 7.0

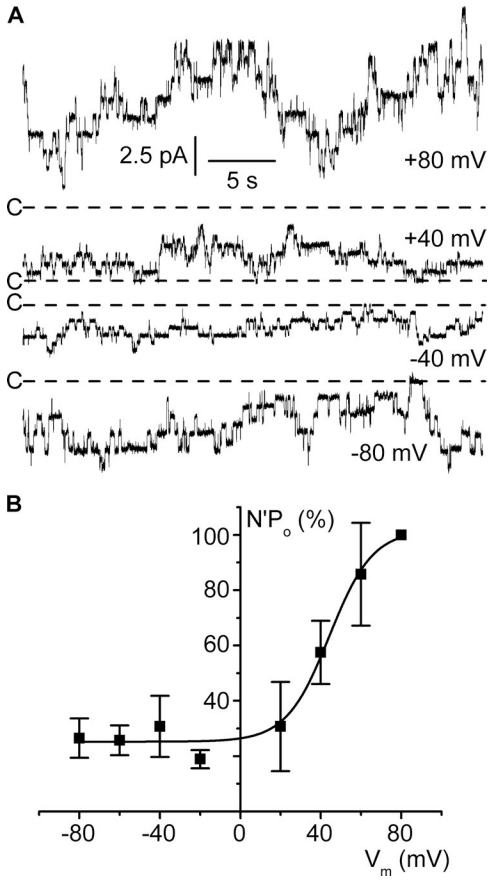

Figure 2. **Channel voltage dependence in the cell-excised inside-out configuration.** Experiments were performed under symmetrical NMDG-Cl conditions (pH 7.4), and pipette solution contained 5 mM Ca^{2+} and bath solution was calcium free. (A) Representative current recordings at the V_m values are given on the right side of each trace. The dashed lines indicate the closed channel current levels (C-). Channel unitary conductance and reversal potential in these conditions (pH_i 7.4) are given in Table S1. (B) Mean $N'P_o/V_m$ relationship. $N'P_o$ data were normalized to the respective $N'P_o$ at V_m 80 mV. Each point is the mean of 6–10 measurements, and SEM is shown as error bars. The continuous line is a nonlinear least squares fit with the Boltzmann equation of mean normalized data.

Published August 29, 2016

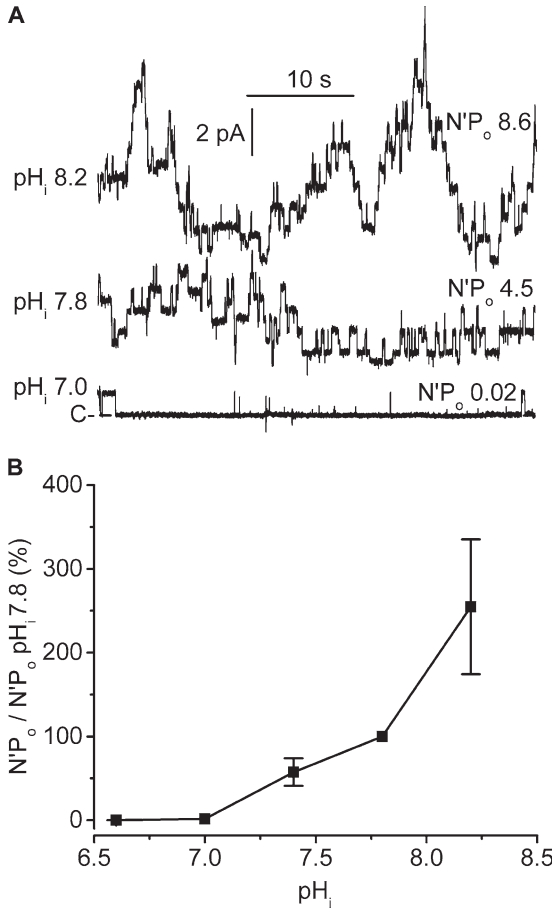

Figure 3. **Dose–response curve for the effects of pH_i on channel activity.** Experiments were performed on cell-excised inside-out membrane patches under symmetrical NMDG-Cl conditions, at V_m 80 mV. Pipette solution contained 5 mM Ca^{2+} (pH_o 7.4), and the bath solution was calcium free. (A) Current traces from the same patch exposed to pH_i 7.0–8.2. For clarity, the traces were superimposed, the dashed line indicating the closed channel current level (C-). The respective $N'P_o$ values are given on the right side of each trace. (B) Dose–response relationship. Each $N'P_o$ value at a given pH_i was normalized to the paired $N'P_o$ at pH_i 7.8 on the same patch. Data are means of measurements from four to five patches, and SEM is given as error bars when larger than symbols.

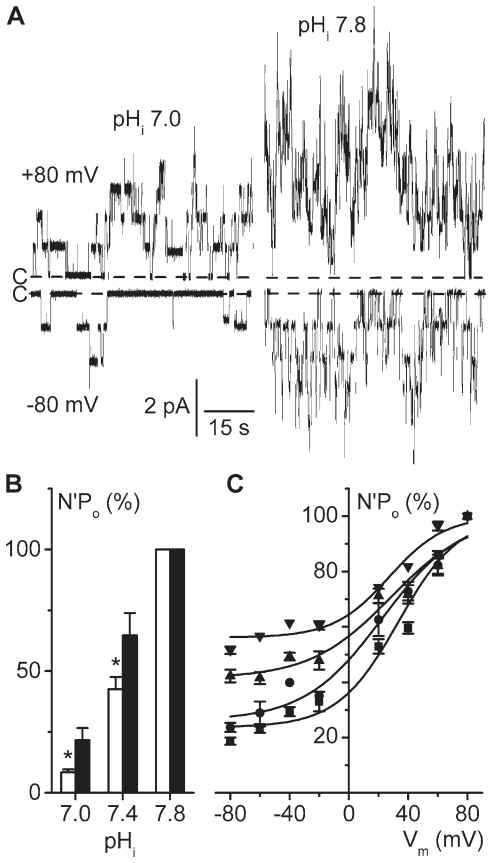

Figure 4. **Increased pH_i flattens the voltage dependence curve.** Experiments were performed on inside-out patches symmetrically bathed in NMDG-Cl solution. Pipette solution contained 5 mM Ca^{2+} (pH 7.4), and the bath solution was calcium free. (A) Recordings from the same patch at V_m 80 mV or at V_m −80 mV, at pH_i 7.0 or 7.8. Dashed lines indicate the closed channel current levels (C-). (B) Effects of pH_i on $N'P_o$ in the conditions given in A, at V_m −80 mV (white bars) and at V_m 80 mV (black bars), at the indicated pH_i values. At each potential, $N'P_o$ values were normalized to their respective values at pH_i 7.8; data are given as means of five experiments, and SEM is shown as error bars. *, $P < 0.05$ versus V_m 80 mV, paired Student's *t* test. (C) Mean $N'P_o/V_m$ curves at pH_i 7.0 (■), 7.4 (●), 7.6 (▲), and 7.8 (▼). For each pH_i condition, $N'P_o$ data were normalized to the respective $N'P_o$ at V_m 80 mV, and each point is the mean of 9–12 (pH_i 7.0), 16–19 (pH_i 7.4), 6–10 (pH_i 7.6), and 8–12 (pH_i 7.8) measurements. SEM is shown as error bars when larger than symbols. Continuous lines are the Boltzmann fits of mean data.

to 7.8 produced qualitatively similar increases in activity at V_m 80 mV and V_m −80 mV (Fig. 4 A), without altering single-channel conductive properties (Table S1). Nevertheless, variations in pH_i at V_m −80 mV elicited a significantly more pronounced effect on $N'P_o$ than at V_m 80 mV (Fig. 4 B), revealing a modulation of voltage dependence. Indeed, $N'P_o/V_m$ curves established at various pH_i values within the 7.0–7.8 range (Fig. 4 C) showed a progressive flattening of the voltage dependence curve with internal alkalinization. Statistical analysis of mean parameters derived from Boltzmann fits of these experimental $N'P_o/V_m$ data revealed that internal alkalinization significantly increased $N'P_o$ at negative voltage without affecting K and $V_{1/2}$ values (Table 1).

Alkaline pH_o shifts the voltage dependence curve toward negative voltages

The effects of pH_o, a known regulator of recombinant and native ClC-K2 channels (Waldegger and Jentsch, 2000; Estévez et al., 2001; Lourdel et al., 2003; Nissant et al., 2006), on voltage dependence were similarly investigated by comparing activities in separate patches when external (pipette) pH was set at either 6.6 or 8.0. Single-channel conductive properties were not affected by pH_o (Table S1), but channel activity clearly increased with positive membrane voltage in both pH_o conditions

Published August 29, 2016

Table 1. **Effects of pH_i, pH_o, and $[Ca^{2+}]_o$ on channel $N'P_o/V_m$ relationships**

Condition	K	$V_{1/2}$	$N'P_o$ min	$N'P_o$ max	R^2
	mV	*mV*	*%*	*%*	
pH_i 7.0 (5)	20.8 ± 3.9	41.7 ± 8.4	19.4 ± 6[a]	111.0 ± 8.2	0.961 ± 0.027
pH_i 7.4 (7)	19.0 ± 6.1	28.8 ± 8.4	19.6 ± 4.5[a]	106.7 ± 8.2	0.905 ± 0.022
pH_i 7.6 (5)	22.9 ± 10.1	29.6 ± 5.9	38.4 ± 11.3	106.4 ± 4.4	0.953 ± 0.016
pH_i 7.8 (5)	20.4 ± 4.6	32.8 ± 4.9	47.3 ± 3.3[a]	104.8 ± 1.7	0.945 ± 0.069
pH_o 6.6 (5)	19.5 ± 6.2	58.0 ± 5.1[b]	33.1 ± 3.3	124.1 ± 12	0.934 ± 0.016
pH_o 7.4 (5)	13.1 ± 2.4	33.0 ± 8.5	35.0 ± 3	105.0 ± 3.2	0.890 ± 0.03
pH_o 8.0 (4)	23.3 ± 6.5	20.8 ± 4.6	37.0 ± 4.5	109.8 ± 3	0.927 ± 0.04
$[Ca^{2+}]_o$ 0 mM (5)	21.2 ± 5.1	34.3 ± 12.6	10.4 ± 2.5	119.5 ± 11.2	0.979 ± 0.015
$[Ca^{2+}]_o$ 5 mM (4)	29.1 ± 5.1	31.4 ± 11.3	6.9 ± 5.3	118.7 ± 11.8	0.965 ± 0.012

Mean parameters from Boltzmann fits (see Materials and methods) of individual $N'P_o/V_m$ relationships in the cell-excised inside-out configuration in the conditions given in the left column. In each condition, $N'P_o$ values were normalized to their respective values at V_m 80 mV. Data are given as means ± SEM for the number of fits indicated in parentheses. For each condition, a measure of the goodness of fit (R^2) is also given. One-way ANOVA revealed significant differences between the $N'P_o$min means of pH_i groups ($P < 0.005$) and between the $V_{1/2}$ means of pH_o groups ($P < 0.01$). Parameters under 0 and 5 mM $[Ca^{2+}]_o$ were not statistically different (unpaired Student's *t* test).

[a]$P < 0.01$ versus pH_i 7.8 (Holm-Šidák multiple comparison procedure).

[b]$P = 0.02$ versus pH_o 8.0 (Holm-Šidák multiple comparison procedure).

(Fig. 5 A). Mean $N'P_o/V_m$ curves established at pH_o 6.6, 7.4, and 8.0 (Fig. 5 B) show that, in contrast with pH_i, increased pH_o did not modify the shape of the curve but caused a significant shift toward less depolarizing voltages by decreasing $V_{1/2}$ (Table 1). A plot of $V_{1/2}$ values from Table 1 as a function of pH_o revealed a ∼12-mV per e-fold change in the external H^+ concentration (Fig. 5 C).

Extracellular calcium concentration ($[Ca^{2+}]_o$) has no influence on ClC-K2 voltage dependence

Experiments were then conducted to assess the impact of variations in $[Ca^{2+}]_o$, by comparing recordings obtained from separate inside-out patches with either a nominally calcium-free or 5 mM calcium–containing pipette solution. $[Ca^{2+}]_o$ had no influence on single-channel conductive properties (Table S1), and channel activity increased with membrane depolarization under each $[Ca^{2+}]_o$ condition (Fig. 6 A). As shown in Fig. 6 B, $[Ca^{2+}]_o$ had no influence on channel voltage dependence, the $N'P_o/V_m$ relationships obtained under each $[Ca^{2+}]_o$ condition being superimposed and Boltzmann fits of experimental $N'P_o/V_m$ curves in each condition yielding similar parameters (Table 1).

Altogether, our results show that pH_i and pH_o, but not $[Ca^{2+}]_o$, modify ClC-K2 channel voltage dependence in such a way that its activity at negative membrane voltages is increased by alkaline pH.

The number of active ClC-K2 channels per patch is critically dependent on pH_i, whereas the effect on P_o is less important

When examining the traces shown in Figs. 3 and 4, it is clear that alkaline pH_i dramatically increases the apparent number of active channels per patch. This suggests a second possible pH_i-dependent modulation of channel activity.

To investigate this issue, we analyzed long-lasting current recordings on patches undergoing successive changes in pH_i without showing noticeable rundown. Fig. 7 A shows a typical channel recording at V_m 80 mV (i.e., under high activity conditions) where pH_i was lowered from 7.4 to 7.0 and then raised back to 7.4. Here, a large reduction in steady-state currents occurred when switching pH_i from 7.4 ($N'P_o$ = 7.96) to 7.0 ($N'P_o$ = 0.96), which was fully reversible when switching back to 7.4 ($N'P_o$ = 10.2). A further rise in pH_i to 7.8 resulted in a huge increase in $N'P_o$ to 28.3. It is also apparent from Fig. 7 A that the changes in activity when switching to different pH_i are quite slow, as illustrated by the ∼1-min lag needed to reach a new steady-state after switching pH_i from 7.4 to 8. We further explored this observation by examining the time course of $N'P_o$ change upon a large and sudden change in pH_i at V_m 80 mV (Fig. 7 B). Here, up to ∼21 channels were simultaneously active at pH_i 7.8, and decreasing pH_i to 6.8 progressively reduced channel activity, reaching a new steady-state with only five active channels within ∼40 s. Based on the mean of four similar experiments, the fit of relaxation current data to a single exponential equation yielded a time constant of 13.6 ± 4.6 s, demonstrating the presence of a slow component in the channel dependence on pH_i.

Recordings obtained at V_m 80 mV and over the 7.4–8.2 pH_i range with sufficiently high activities enabled us to estimate N' and P_o values from peak activity measurements in good agreement with results from stationary noise analysis (see Materials and methods). As illustrated in Fig. 7 C, the increase in $N'P_o$ with pH_i was caused by a dramatic increase in N' over the 7.4–8.2 pH_i range, associated (pH_i 7.4–7.8) or not (pH_i 7.8–8.2) with a moderate increase in P_o.

pH_o and $[Ca^{2+}]_o$ also modulate the number of active ClC-K2 channels per patch

In cell-attached patches from DCT cells, the effects of pH_o and of $[Ca^{2+}]_o$ on ClC-K2 channels were similarly related to a major modulation in the number of

Published August 29, 2016

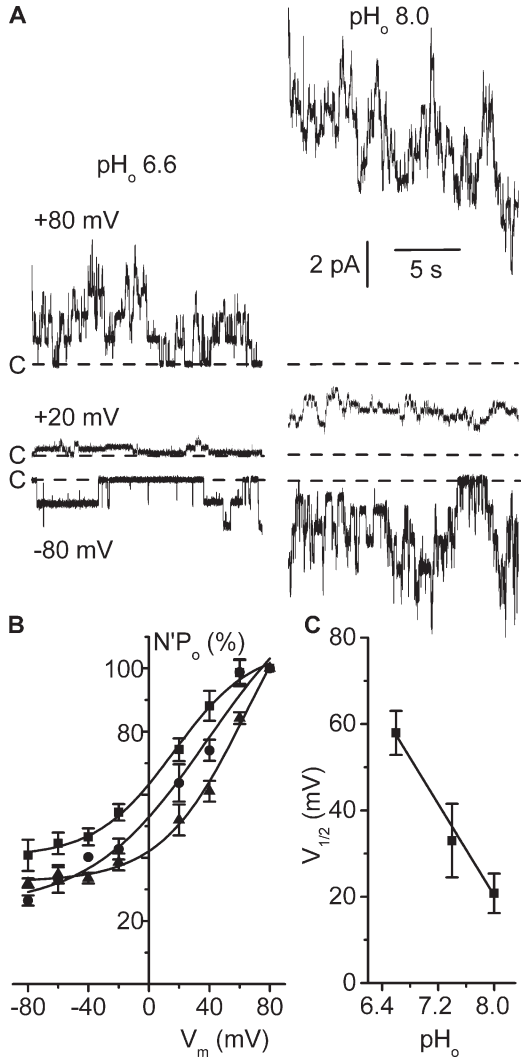

Figure 5. **Variations in pH_o shift the voltage dependence curve.** Experiments were performed on inside-out patches symmetrically bathed in NMDG-Cl solution. Pipette solution contained 5 mM Ca^{2+}, and the bath solution was calcium free and adjusted at pH 7.4. (A) Current recordings from two separate patches under external (pipette) pH, pH_o, 6.6 (left traces) or 8.0 (right traces) and clamped at the V_m values given on the left side. The dashed lines indicate the closed channel current levels (C-). (B) Mean $N'P_o/V_m$ relationships at pH_o 6.6 (▲), 7.4 (●), and 8.0 (■). For each pH_o condition, $N'P_o$ data were normalized to the respective value at V_m 80 mV. Each point is the mean of 5 (pH_o 6.6 and 8.0) or 6 (pH_o 7.4) measurements, and SEM is shown as error bars when larger than symbols. Continuous lines are nonlinear least squares fits of respective mean data with the Boltzmann equation. (C) Mean $V_{1/2}$ values from Table 1 plotted as a function of pH_o, and SEM is shown as error bars. Data were fitted by a straight line with a slope of 26.6 ± 1.99 mV/pH_o unit (R^2 = 0.989).

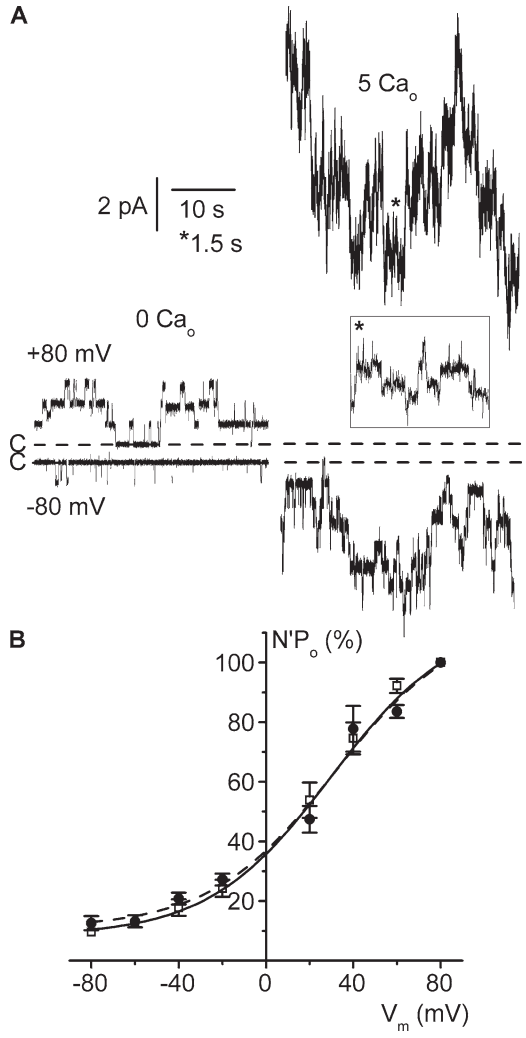

Figure 6. **$[Ca^{2+}]_o$ does not affect channel voltage dependence.** Experiments were performed on cell-excised inside-out membrane patches symmetrically bathed in NMDG-Cl solution (pH 7.4) and under calcium-free bath solution. (A) Representative current recordings from two separate patches clamped at V_m 80 mV (top traces) or −80 mV (bottom traces) and under calcium-free (0 Ca_o, left) or 5 mM (5 Ca_o, right) external (pipette) conditions. The dashed lines indicate the closed channel current levels (C-). The inset is an excerpt of the trace at V_m 80 mV taken at the indicated location (asterisk) with the corresponding expanded time scale. (B) Mean $N'P_o/V_m$ relationships under external calcium-free (□) or 5 mM Ca^{2+} (●) condition. For each $[Ca^{2+}]_o$ condition, $N'P_o$ data were normalized to the respective $N'P_o$ value at V_m 80 mV. Each point is the mean of five measurements, and SEM is shown as error bars when larger than symbols. Continuous and dashed lines are nonlinear least squares fits with the Boltzmann equation of calcium-free and 5 mM Ca^{2+} mean data, respectively.

active channels (Lourdel et al., 2003). Fig. S4 shows that modulation by pH_o and $[Ca^{2+}]_o$ was also seen in cell-excised patches from CNT cells. Here, $N'P_o$ was measured during the first 2 min after excision of separate patches under various pH_o or $[Ca^{2+}]_o$ conditions, at V_m 80 mV. In these conditions, the high $N'P_o$ at pH_o 8.0, as compared with that on separate patches at pH_o 6.6, was caused by a dramatic increase in N′ and by a moderate, yet significant, increase in P_o (Fig. S4 A), possibly by the pH_o-dependent shift in voltage dependence (see previous section). Similarly, the high $N'P_o$

Published August 29, 2016

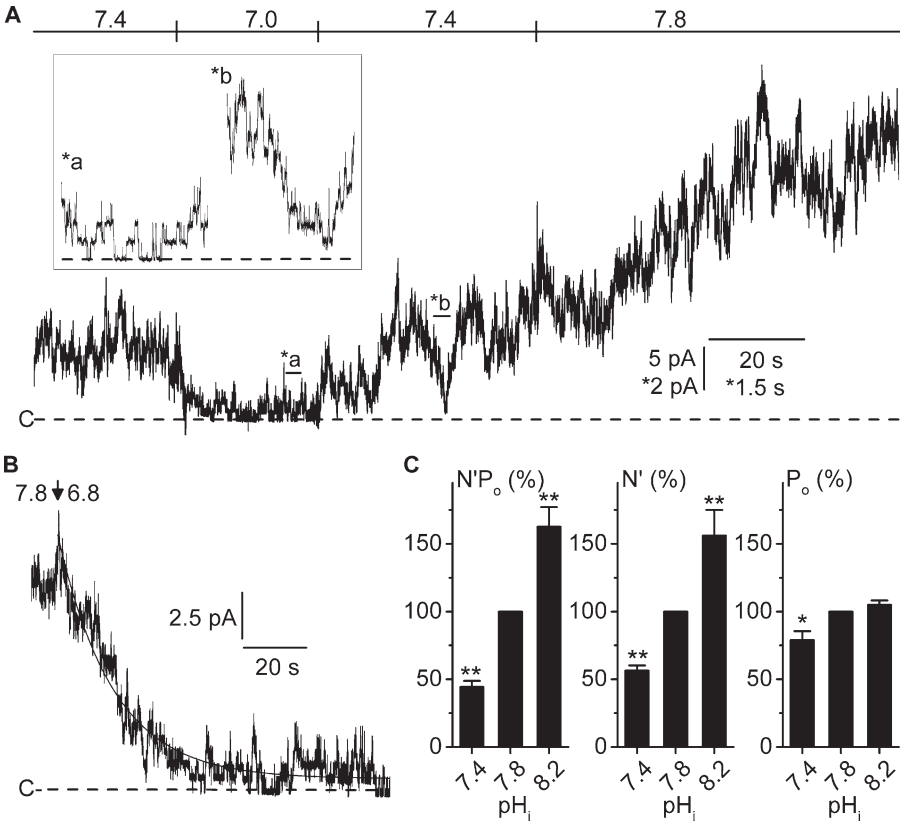

Figure 7. **pH$_i$ modulates the number of active channels.** (A) Representative continuous current recording from an inside-out membrane patch at V_m 80 mV, symmetrically bathed in NMDG-Cl solution. Pipette solution contained 5 mM Ca^{2+} (pH 7.4), and pH$_i$ was varied as indicated. The inset contains two excerpts taken at the indicated locations (a and b) at the expanded time and amplitude scales (*). The dashed lines indicate the closed channel current levels (C-). (B) Time course of the change in channel activity upon switching pH$_i$ from 7.8 to 6.8 (arrow), at V_m 80 mV. The dashed line indicates the closed channel current level (C-). The fit of the trace under pH$_i$ 6.8 to a single exponential equation (continuous line) indicated an e-fold decrease in channel activity after 17.1s. (C) N′P$_o$, number of active channels (N′) and P$_o$ as a function of pH$_i$. Paired data were obtained as described in A and normalized to the respective value at pH$_i$ 7.8. N′ was determined by peak current measurements and validated by stationary noise analysis (see Materials and methods). Only recordings yielding ΔN′/N′ values within the 95% agreement interval were taken as valid. Data are given as means from four patches, and SEM is shown as error bars. N′P$_o$, N′, and P$_o$ means significantly were affected by pH$_i$ ($P < 0.001$, $P < 0.001$, and $P = 0.005$, respectively; one-way ANOVA). **, $P < 0.001$; and *, $P < 0.02$ versus pH$_i$ 7.8 (Holm-Šidák multiple comparison procedure).

observed under 5 mM external Ca^{2+} as compared with Ca^{2+}-free conditions could be related to an increase in N′, whereas no significant change in P$_o$ was observed (Fig. S4 B).

Voltage affects both the number of active channels and P$_o$, but alkaline pH$_i$ blunts the voltage dependence by acting on P$_o$ only

We first evaluated the time course of the change in channel activity upon sudden variations in V_m. As illustrated in Fig. 8 A, switching V_m from 80 to −80 mV caused an initial peak in channel activity followed by a progressive decay. The relaxation currents could be fitted to a single exponential equation with time constants of 18.7 ± 4 s after a 80 to −80-mV transition ($n = 12$) and of 19.6 ± 7.6 s for a −80 to 80-mV transition ($n = 6$), indicating the involvement of a relatively slow component in the channel dependence on voltage.

We then evaluated N′ and P$_o$ at positive and negative membrane voltages. For this purpose, we selected a subset of data compatible with an analysis of N′ and P$_o$ as defined in the Materials and methods section, in which recordings were obtained at V_m 80, 40, −40, and −80 mV from the same patch ($n = 5$). Under these specific conditions, we observed a major increase in N′ with depolarization ($P = 0.007$, one-way ANOVA), but also a moderate but significant ($P = 0.023$, one-way ANOVA) increase in P$_o$ (Fig. 8 B).

To investigate how pH$_i$ modulates the channel voltage dependence illustrated in Fig. 4, we analyzed another subset of data comprising N′P$_o$, N′, and P$_o$ measurements at pH$_i$ 7.4 and 7.8 and at V_m 80 and −80 mV, in the same patch. As shown in Fig. 8 C, at pH 7.4, the profound decrease in N′P$_o$ observed at −80 mV (as compared with N′P$_o$ at 80 mV) was related to significant reductions in both N′ (by ∼65%, middle panel) and P$_o$ (by ∼35%, right panel). In contrast, at pH 7.8, the less pronounced decrease in N′P$_o$ observed at −80 mV was purely caused by a reduction in N′ (by ∼50%) without any variation of P$_o$. We may conclude that the effect of pH$_i$ on voltage dependence includes two components, a dominant N′ modulation, which can be detected over a large range of pH$_i$ values, and a modest P$_o$ modulation, apparent only at pH$_i$ ≤ 7.4.

Published August 29, 2016

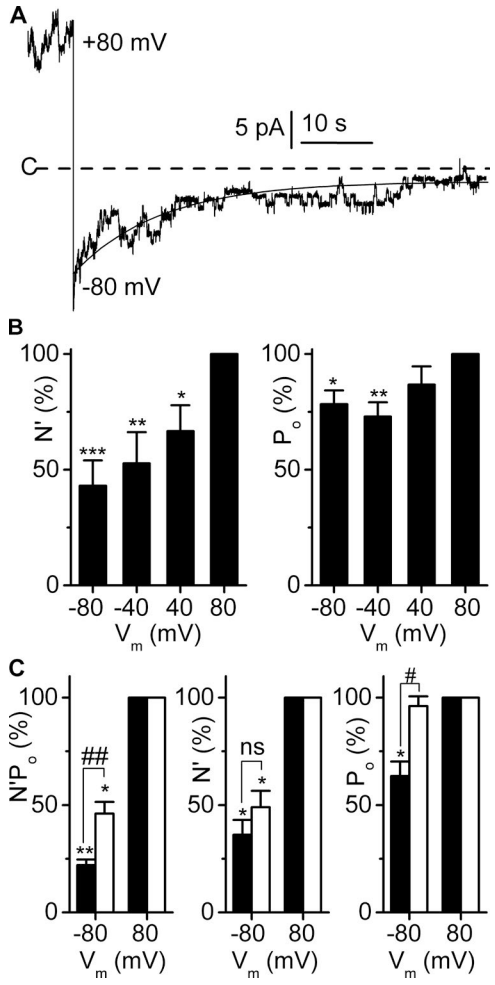

Figure 8. **Membrane voltage modulates the open probability and the number of active channels.** Experiments were performed on cell-excised inside-out membrane patches symmetrically bathed in NMDG-Cl solution. Pipette solution contained 5 mM Ca^{2+} (pH_o 7.4), and bath solution was calcium free. (A) Time course of the change in channel activity upon switching V_m from 80 to −80 mV, at pH_i 7.4. The dashed line indicates the closed channel current level (C-). The fit of the trace at V_m −80 mV to a single exponential equation (continuous line) indicated an e-fold decrease in channel activity within ∼15 s. (B) Number of active channels per patch (N′) and P_o as a function of V_m. For each patch, paired data were normalized to the respective value at V_m 80 mV, pH_i 7.4. *, $P < 0.05$; **, $P = 0.01$; and ***, $P < 0.005$, versus V_m 80 mV (Holm-Šidák multiple comparison procedure). (C) Modulation by pH_i of the effects of V_m on N′ and P_o. For each patch, paired data at pH_i 7.4 (black bars) or 7.8 (white bars), at V_m −80 mV, were normalized to the respective value at V_m 80 mV. *, $P < 0.005$; ** $P < 0.0001$, versus V_m 80 mV; and #, $P < 0.05$; ##, $P < 0.005$ versus pH_i 7.8, paired Student's *t* test. (B and C) Data are given as means from five patches, and SEM is shown as error bars. N′ was determined by peak current measurements and validated by stationary noise analysis (see Materials and methods). Only recordings yielding ΔN′/N′ values within the 95% agreement interval were taken as valid.

Modeling ion transport in type B intercalated cells

Even though ClC-K2 channels are densely present in the basolateral membrane, only a small fraction of these channels is active under physiological conditions (i.e., at pH 7.4 and negative membrane voltage). Furthermore, pH-dependent processes (acting via external and internal pH) around physiological values powerfully modulate ClC-K2 activity, implying that the basolateral chloride conductance (i.e., gClC-K) can change dramatically under conditions of acidosis or alkalosis (from nearly 0% at pH_o 7.0 to 100% around pH_o 8.2, changes in pH_o are accompanied by parallel changes in pH_i). For this reason, we wished to evaluate how gClC-K modulation might affect ion transport in type B intercalated cells. Type B intercalated cells are classically involved in HCO_3^- secretion (Staruschenko, 2012), but the group of Eladari and Chambrey (Leviel et al., 2010; Chambrey et al., 2013; Eladari et al., 2014) more recently showed that these cells are also able to reabsorb NaCl through an electroneutral process. The net reabsorption of NaCl is energized by basolateral V-ATPase pumps. Na^+ enters the cell on the apical side via the Na^+-driven Cl^-/HCO_3^- exchanger NDCBE and exits via the Na^+-HCO_3^- transporter AE4 on the basolateral side. The apical uptake of Cl^- is mediated by the Cl^-/HCO_3^- exchanger pendrin; a fraction of Cl^- is recycled via NDCBE, whereas the remainder exits via the basolateral Cl^- channel ClC-K2 (Fig. 9 A).

We modeled ion transport in type B intercalated cells by integrating these main ion transport systems (see Materials and methods) and evaluated Na^+, Cl^-, and HCO_3^- transport under asymmetric conditions, i.e., with a low NaCl concentration in the lumen. When the basolateral gClC-K is maximal (a condition possibly corresponding to strong alkalosis), there is a large transepithelial Cl^- flux associated with a minimal Na^+ flux (Fig. 9 A): in these conditions, the intercalated cells exchange HCO_3^- for Cl^- but do not reabsorb Na^+ (Fig. 9 B). Reducing progressively gClC-K switches the intercalated cell to a NaCl-transporting system (Fig. 9 B): when gClC-K is ∼15% of its maximal value (corresponding to resting pH conditions), the transepithelial Cl^- flux is only coupled to the Na^+ flux. Finally, at very low gClC-K (such as in acidotic conditions), the Cl^- flux tends toward zero and Na^+ is absorbed with HCO_3^-. These simulations suggest that the basolateral Cl^- conductance is a critical ion transport parameter in the type B intercalated cell, whose modulation allows switching between several modes of transport.

DISCUSSION

Previous single-channel patch clamp analyses on wild-type and *Clcnk2*$^{-/-}$ mice have established that the major basolateral Cl^- channel along the distal nephron is a ∼10-pS Cl^- channel formed by ClC-K2 (Lourdel et al., 2003; Nissant et al., 2004, 2006; Zaika et al., 2015). The present study focused on the regulation of the native renal ClC-K2 by characteristic modulators of ClC chan-

Published August 29, 2016

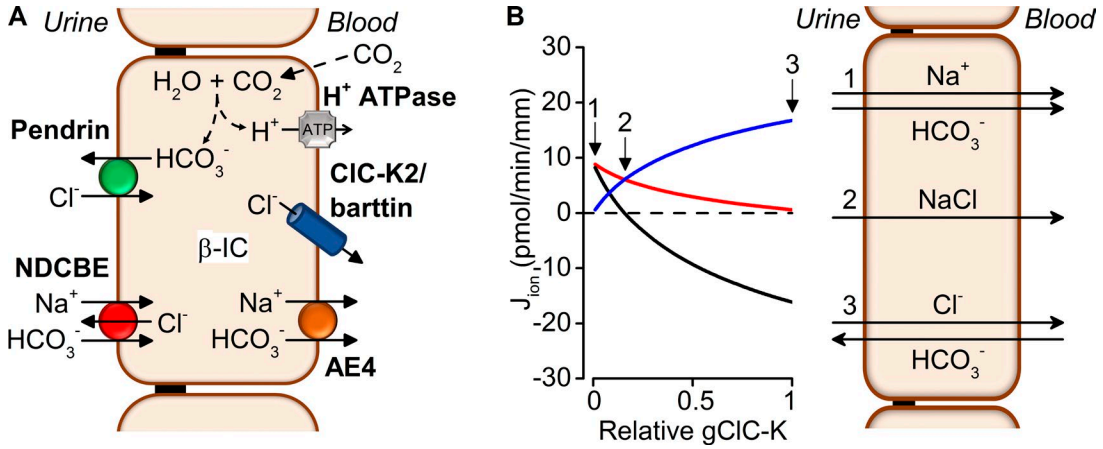

Figure 9. **Modeling ion transport in the type B intercalated cells.** (A) Ion transporter model used for simulations (see Materials and methods). Type B intercalated cells secrete HCO_3^- into the lumen by the apical Cl^-/HCO_3^- exchanger pendrin coupled to the basolateral efflux of protons by the V-ATPase and of Cl^- by the ClC-K2/Barttin channel. Electroneutral NaCl reabsorption is mediated by the apical coupling of pendrin with the Na^+-driven Cl^-/HCO_3^- exchanger NDCBE and by the basolateral extrusion of Na^+ by Na^+-HCO_3^- cotransporter AE4, and of Cl^- by ClC-K2. (B) Predicted effects of variations in basolateral membrane chloride conductance (gClC-K) on net fluxes of Cl^- through ClC-K2 (blue), of Na^+ through NDCBE (red), and of apical HCO_3^- (black; left) and on net transcellular Na^+, Cl^-, and HCO_3^- transport (right). The labels 1–3 correspond to relative gClC-K values of 0, 0.15, and 1, respectively.

nels and describes the key role of external and internal pH synergistically modulating membrane voltage dependence at negative membrane voltages.

Voltage dependence

We first showed that voltage dependence, a general property of ClC Cl^- channels (Uchida and Sasaki, 2005; Jentsch, 2008; Stölting et al., 2014), is also a characteristic of the native renal ClC-K2 channel. Previous studies on the regulation by membrane voltage of recombinant human ClC-Kb provided contradictory information. Two-electrode voltage clamp experiments on ClC-Kb/barttin channels expressed in *Xenopus laevis* oocytes showed time- and voltage-dependent gating, currents activating upon membrane depolarization and deactivating upon membrane hyperpolarization (Estévez et al., 2001; Waldegger et al., 2002; Picollo et al., 2004; Gradogna et al., 2010). In contrast, whole-cell currents from renal HEK and tsA201-cultured cells transfected with ClC-Kb/barttin showed no relaxation component (Estévez et al., 2001; Scholl et al., 2006; Fahlke and Fischer, 2010). There is no clear explanation for this discrepancy, but the similar voltage dependence in cell-attached and cell-excised inside-out membrane patches in our experiments very likely rules out the loss of an unknown intracellular signal regulating gating upon cell dialysis in ClC-Kb/barttin whole-cell measurements. Interestingly, we observed that the native ClC-K2 channel displays slow kinetics with two open states of 0.3 s and 2.2 s and one very long closed state of 6.5 s (Lourdel et al., 2003), and with a relaxation time constant close to 20 s (this study). Such a slow component in ClC-K2 channel gating may have been missed under the short (<500 ms) pulses used in whole-cell studies of recombinant ClC-K2 channels.

Regulation of channel activity by pH and calcium

Regulation by external H^+ and Ca^{2+} is a typical property of all ClC-K channels (Estévez et al., 2001; Waldegger et al., 2002) that was studied in detail by Pusch and associates (Gradogna et al., 2010, 2012; Imbrici et al., 2014). The effects of external H^+ and Ca^{2+} on recombinant ClC-Kb are independent, acting on separate binding sites located at the outer layer of the protein and therefore not indirectly mediated by some regulatory cell component (Gradogna et al., 2010). This is in agreement with our results on the native mouse ClC-K2. We previously demonstrated that the native ~10-pS Cl^- channel in mouse renal tubules was sensitive to external H^+ and Ca^{2+} in cell-attached patches (Lourdel et al., 2003; Nissant et al., 2006). We show here that this property can still be observed in excised patches, ruling out the hypothesis that the effects of pH_o are in fact caused by secondary changes in pH_i. In contrast to the well-recognized effects of pH_o, pH_i effects have never been investigated on recombinant ClC-K channels and may not be a general property of ClC-K channels. Indeed, a ~45-pS Cl^- channel in mouse TAL (Paulais and Teulon, 1990), later identified as ClC-K1 (L'Hoste et al., 2013), the murine orthologue of ClC-Ka in humans, was shown to be hardly sensitive to this parameter. There is presently no clue regarding the mechanism responsible for ClC-K2 pH_i sensitivity. Further investigations on recombinant ClC-K2 would be necessary to determine the presence of a specific binding site for intracellular H^+. Two facts are worth mentioning: (1) quite puzzlingly, the pKa for pH_i effects is very alkaline, as is that for pH_o effects in ClC-Kb (Gradogna et al., 2010; Andrini et al., 2015); (2) although pH_i affects mainly the number of active channels over a large range of pH_i,

Published August 29, 2016

there is clearly a more rapid component affecting P_o at negative membrane voltages that can be detected at $pH_i \leq 7.4$. This suggests that pH_i might be acting via two distinct mechanisms.

ClC complex gating

The ClC channels are functional dimers, whose activity is controlled by two independent processes, the two independent protopore gates and the common gate that simultaneously opens/closes the two protopores (Pusch, 2004; Chen, 2005; Jentsch, 2008). The protopore gating involves the protonation/deprotonation of a glutamate residue at position 166. In contrast, the mechanisms of the common gate have not yet been elucidated; it functions as an inactivation process driven by depolarization in ClC-0 and ClC-2 channels and by hyperpolarization in the ClC-1 channel. It can be very slow (tens of seconds), as in ClC-0, or relatively fast (hundreds of milliseconds), as in ClC-1 (Pusch, 2004; Chen, 2005; Jentsch, 2008). Because the ClC-K channels lack the characteristic glutamate residue involved in the protopore gate mechanism of ClC channels, ClC-K channel gating is presumed to be controlled mainly by the common gate. Accordingly, the protopore conductance is only rarely detected under the form of short-lived, half-openings for the native ClC-K2 (Lourdel et al., 2003) and recombinant mouse ClC-K1 (L'Hoste et al., 2013) channels, whereas it is clearly observed after insertion of a glutamate at position 166 in mouse ClC-K1 (L'Hoste et al., 2013). Likewise, in the present experiments, we did not notice more frequent half-openings under specific conditions of membrane voltage, pH, or Ca^{2+} concentration. In sum, this suggests that ClC-K2 gating is dominated by the common gate.

Mechanisms involved in ClC-K2 regulation

The effects of $[Ca^{2+}]_o$, pH_i and pH_o appear to be mainly caused by variations in the apparent number of active ClC-K2 channels. The presence of separate binding sites for Ca^{2+} and H^+ at the outer side of the ClC-Ka protein (Gradogna et al., 2010), a ClC-Kb isoform, makes it unlikely that changes in the total number of channels in cell-attached membrane patches, via channel trafficking to and from the membrane, may have modulated the number of channels after changes in the external environment (i.e., $[Ca^{2+}]_o$ or pH_o). In cell-excised membrane patches, it can be reasonably admitted that the total number of channel proteins per patch remains constant upon changes in pH_i, i.e., we may discard the possibility that trafficking processes are involved in this regulation. Nevertheless, the actual number of active channels in the patch membrane may fluctuate during the whole duration of the current recording, either because some of the channels present in the patch spontaneously enter a "sleepy" (inactive) state or because regulatory factors favor an inactivated state (Colquhoun and Hawkes, 1995). We propose that, under acid pH_i conditions, a fraction of the channels present in the membrane patch enter into an electrically quiescent state and do not contribute to the pool of electrically active channels over a time scale of tens of seconds (which represents the time scale of our recordings). According to this hypothesis, conformational changes upon increased $[Ca^{2+}]_o$ would stabilize the channel in an activated mode, increasing the number of active channels on the membrane patch, whereas H^+, in contrast, would stabilize the channel in an inactivated state and increase the number of electrically quiescent channels.

Voltage dependence can also be explained within the same framework, membrane hyperpolarization favoring an inactivated state and decreasing the apparent number of active channels. However, it is clear from our results that P_o is a second voltage-dependent component. The modulation of P_o with voltage, as illustrated in Fig. 7 B, is modest, with a decrease of ∼25–30% at −80 mV compared with 80 mV at pH 7.4. P_o modulation disappears at pH 7.8, suggesting that protons might interfere with common gating, possibly via an intracellular site distinct from the one modulating N′. The effect of pH_i on P_o is not limited to negative voltages but is also observed at positive voltages when pH_i is decreased to 7.4.

Therefore, we suggest that the activity of the native ClC-K2 channel is modulated by two slow processes, i.e., the open probability and the number of active channels. P_o modulation would correspond to channel common gating stricto sensu and N′ modulation to the channels entering/leaving an inactivated state of long duration. Regarding the latter, abrupt changes in voltage and pH_i interestingly affected channel activity with comparable kinetics (see Figs. 7 B and 8 A), but we cannot rule out that these two factors, and likely pH_o and $[Ca^{2+}]_o$, may indeed modulate N′ by separate mechanisms with similar time constants.

ClC-K2 regulation in the context of renal physiology

The native ClC-K2 is present at very high density in the basolateral membranes of the distal nephron (Lourdel et al., 2003; Nissant et al., 2006). Our previous (Lourdel et al., 2003; Nissant et al., 2006) and present results indicate that the number of active (detectable) channels under physiological conditions of calcium and pH is considerably lower than the actual number of channels present in the patch (as evaluated with alkaline pH or elevated calcium). Thus, we may envision the ClC-K2 channel population as a large reservoir of silent channels in the basolateral membranes, which may be mobilized by regulatory factors. Our results show that $[Cl^-]_i$ may not be viewed as a physiological regulator of ClC-K2, whereas the intracellular and pH_o might be key regulators of ClC-K2 under diverse acido-basic conditions,

as pH_o variations should induce smaller but parallel variations in pH_i.

Our modeling study gives some insight into the conditions of ion transport in type B intercalated cells. When the basolateral Cl^- conductance is maximal, type B intercalated cells mostly exchange HCO_3^- for Cl^-, fulfilling their primary function of HCO_3^- excretion, without absorbing Na^+. This prediction results from the fact that the Cl^- gradient across the apical membrane is not favorable to the uptake of Na^+ via NDCBE, whereas the high basolateral Cl^-conductance optimizes the recirculation of the Cl^- ions entering the cell by means of the Pendrin exchanger. When the Cl^- conductance is reduced to 15% or more of its maximal value, the ClC-K2–mediated Cl^- flux is decreased but it is now accompanied by a parallel Na^+ transcellular flux. In sum, under low luminal NaCl conditions, variations in basolateral Cl^- conductance may switch type B intercalated cells from a state where they primarily exchange HCO_3^- against Cl^- to a state where NaCl transport is favored. Thus, we suggest that pH, by controlling ClC-K2 activity, is in a position to decrease Na^+ absorption across type B intercalated cells while stimulating Cl^-/HCO_3^- exchange during alkalosis.

Of course, given the involvement of ClC-K2 in renal NaCl absorption, it would be attractive to link Cl^- channel modulation to hormones and mediators (Wu et al., 2013; Zaika et al., 2015). Future studies are needed to investigate whether these regulations are also acting on the number of active channels either via phosphorylation/dephosphorylation processes of the channel (Zaika et al., 2015) or via variations in the pH_i that may alter the transport status of intercalated cells.

ACKNOWLEDGMENTS

The English text was edited by Charlotte Sumida.

This work was supported by grants from the French National Research Agency (ANR-14-CE12-0013-02).

The authors declare no competing financial interests.

Merritt Maduke served as editor.

Submitted: 18 May 2016
Accepted: 7 July 2016

REFERENCES

Andrini, O., M. Keck, S. L'Hoste, R. Briones, L. Mansour-Hendili, T. Grand, F.V. Sepúlveda, A. Blanchard, S. Lourdel, R. Vargas-Poussou, and J. Teulon. 2014. *CLCNKB* mutations causing mild Bartter syndrome profoundly alter the pH and Ca^{2+} dependence of ClC-Kb channels. *Pflugers Arch.* 466:1713–1723. http://dx.doi.org/10.1007/s00424-013-1401-2

Andrini, O., M. Keck, R. Briones, S. Lourdel, R. Vargas-Poussou, and J. Teulon. 2015. ClC-K chloride channels: emerging pathophysiology of Bartter syndrome type 3. *Am. J. Physiol. Renal Physiol.* 308:F1324–F1334. http://dx.doi.org/10.1152/ajprenal.00004.2015

Beck, F.X., A. Dörge, R. Rick, M. Schramm, and K. Thurau. 1988. The distribution of potassium, sodium and chloride across the apical membrane of renal tubular cells: effect of acute metabolic alkalosis. *Pflugers Arch.* 411:259–267. http://dx.doi.org/10.1007/BF00585112

Bland, J.M., and D.G. Altman. 1999. Measuring agreement in method comparison studies. *Stat. Methods Med. Res.* 8:135–160. http://dx.doi.org/10.1191/096228099673819272

Chambrey, R., I. Kurth, J. Peti-Peterdi, P. Houillier, J.M. Purkerson, F. Leviel, M. Hentschke, A.A. Zdebik, G.J. Schwartz, C.A. Hübner, and D. Eladari. 2013. Renal intercalated cells are rather energized by a proton than a sodium pump. *Proc. Natl. Acad. Sci. USA.* 110:7928–7933. http://dx.doi.org/10.1073/pnas.1221496110

Chen, T.Y. 2005. Structure and function of clc channels. *Annu. Rev. Physiol.* 67:809–839. http://dx.doi.org/10.1146/annurev.physiol.67.032003.153012

Chen, M.F., and T.Y. Chen. 2001. Different fast-gate regulation by external Cl^- and H^+ of the muscle-type ClC chloride channels. *J. Gen. Physiol.* 118:23–32. http://dx.doi.org/10.1085/jgp.118.1.23

Colquhoun, D., and A.G. Hawkes. 1995. The principle of the stochastic interpretation of ion-channel mechanisms. *In* Single-Channel Recordings. Second edition. B. Sakmann and E. Neher, editors. Springer, New York. 397–482.

Eladari, D., R. Chambrey, N. Picard, and J. Hadchouel. 2014. Electroneutral absorption of NaCl by the aldosterone-sensitive distal nephron: implication for normal electrolytes homeostasis and blood pressure regulation. *Cell. Mol. Life Sci.* 71:2879–2895. http://dx.doi.org/10.1007/s00018-014-1585-4

Estévez, R., T. Boettger, V. Stein, R. Birkenhäger, E. Otto, F. Hildebrandt, and T.J. Jentsch. 2001. Barttin is a Cl^- channel β-subunit crucial for renal Cl^- reabsorption and inner ear K^+ secretion. *Nature.* 414:558–561. http://dx.doi.org/10.1038/35107099

Fahlke, C. 2001. Ion permeation and selectivity in ClC-type chloride channels. *Am. J. Physiol. Renal Physiol.* 280:F748–F757.

Fahlke, C., and M. Fischer. 2010. Physiology and pathophysiology of ClC-K/barttin channels. *Front. Physiol.* 1:155. http://dx.doi.org/10.3389/fphys.2010.00155

Fischer, M., A.G.H. Janssen, and C. Fahlke. 2010. Barttin activates ClC-K channel function by modulating gating. *J. Am. Soc. Nephrol.* 21:1281–1289. http://dx.doi.org/10.1681/ASN.2009121274

Gradogna, A., E. Babini, A. Picollo, and M. Pusch. 2010. A regulatory calcium-binding site at the subunit interface of CLC-K kidney chloride channels. *J. Gen. Physiol.* 136:311–323. http://dx.doi.org/10.1085/jgp.201010455

Gradogna, A., C. Fenollar-Ferrer, L.R. Forrest, and M. Pusch. 2012. Dissecting a regulatory calcium-binding site of CLC-K kidney chloride channels. *J. Gen. Physiol.* 140:681–696. http://dx.doi.org/10.1085/jgp.201210878

Gray, P.T.A. 1994. Analysis of whole cell currents to estimate the kinetics and amplitude of underlying unitary events: relaxation and 'noise' analysis. *In* Microelectrodes Techniques, The Plymouth Workshop Handbook. Second edition. D. Ogden, editor. Company of Biologists, Cambridge, MA. 189–207.

Greger, R., H. Oberleithner, E. Schlatter, A.C. Cassola, and C. Weidtke. 1983. Chloride activity in cells of isolated perfused cortical thick ascending limbs of rabbit kidney. *Pflugers Arch.* 399:29–34. http://dx.doi.org/10.1007/BF00652518

Hennings, J.C., O. Andrini, N. Picard, M. Paulais, A.K. Hübner, I.K. Lopez Cayuqueo, Y. Bignon, M. Keck, N. Cornière, D. Böhm, et al. 2016. The ClC-K2 chloride channel is critical for salt handling in the distal nephron. *J. Am. Soc. Nephrol.*. http://dx.doi.org/10.1681/ASN.2016010085

Imbrici, P., A. Liantonio, A. Gradogna, M. Pusch, and D.C. Camerino. 2014. Targeting kidney CLC-K channels: pharmacological profile in a human cell line versus *Xenopus* oocytes. *Biochim. Biophys. Acta.* 1838:2484–2491. http://dx.doi.org/10.1016/j.bbamem.2014.05.017

Jentsch, T.J. 2008. CLC chloride channels and transporters: from genes to protein structure, pathology and physiology. *Crit. Rev. Biochem. Mol. Biol.* 43:3–36. http://dx.doi.org/10.1080/10409230701829110

Kieferle, S., P. Fong, M. Bens, A. Vandewalle, and T.J. Jentsch. 1994. Two highly homologous members of the ClC chloride channel family in both rat and human kidney. *Proc. Natl. Acad. Sci. USA.* 91:6943–6947. http://dx.doi.org/10.1073/pnas.91.15.6943

Krämer, B.K., T. Bergler, B. Stoelcker, and S. Waldegger. 2008. Mechanisms of disease: the kidney-specific chloride channels ClCKA and ClCKB, the Barttin subunit, and their clinical relevance. *Nat. Clin. Pract. Nephrol.* 4:38–46. http://dx.doi.org/10.1038/ncpneph0689

L'Hoste, S., A. Diakov, O. Andrini, M. Genete, L. Pinelli, T. Grand, M. Keck, M. Paulais, L. Beck, C. Korbmacher, et al. 2013. Characterization of the mouse ClC-K1/Barttin chloride channel. *Biochim. Biophys. Acta.* 1828:2399–2409. http://dx.doi.org/10.1016/j.bbamem.2013.06.012

Leviel, F., C.A. Hübner, P. Houillier, L. Morla, S. El Moghrabi, G. Brideau, H. Hassan, M.D. Parker, I. Kurth, A. Kougioumtzes, et al. 2010. The Na^+-dependent chloride-bicarbonate exchanger SLC4A8 mediates an electroneutral Na^+ reabsorption process in the renal cortical collecting ducts of mice. *J. Clin. Invest.* 120:1627–1635. (published erratum appears in *J. Clin. Invest.* 2011. 121:1668) http://dx.doi.org/10.1172/JCI40145

Lourdel, S., M. Paulais, P. Marvao, A. Nissant, and J. Teulon. 2003. A chloride channel at the basolateral membrane of the distal-convoluted tubule: a candidate ClC-K channel. *J. Gen. Physiol.* 121:287–300. http://dx.doi.org/10.1085/jgp.200208737

Miller, C., and M.M. White. 1980. A voltage-dependent chloride conductance channel from Torpedo electroplax membrane. *Ann. N. Y. Acad. Sci.* 341:534–551. http://dx.doi.org/10.1111/j.1749-6632.1980.tb47197.x

Niemeyer, M.I., L.P. Cid, L. Zúñiga, M. Catalán, and F.V. Sepúlveda. 2003. A conserved pore-lining glutamate as a voltage- and chloride-dependent gate in the ClC-2 chloride channel. *J. Physiol.* 553:873–879. http://dx.doi.org/10.1113/jphysiol.2003.055988

Nissant, A., S. Lourdel, S. Baillet, M. Paulais, P. Marvao, J. Teulon, and M. Imbert-Teboul. 2004. Heterogeneous distribution of chloride channels along the distal convoluted tubule probed by single-cell RT-PCR and patch clamp. *Am. J. Physiol. Renal Physiol.* 287:F1233–F1243. http://dx.doi.org/10.1152/ajprenal.00155.2004

Nissant, A., M. Paulais, S. Lachheb, S. Lourdel, and J. Teulon. 2006. Similar chloride channels in the connecting tubule and cortical collecting duct of the mouse kidney. *Am. J. Physiol. Renal Physiol.* 290:F1421–F1429. http://dx.doi.org/10.1152/ajprenal.00274.2005

Pácha, J., G. Frindt, L. Antonian, R.B. Silver, and L.G. Palmer. 1993. Regulation of Na channels of the rat cortical collecting tubule by aldosterone. *J. Gen. Physiol.* 102:25–42. http://dx.doi.org/10.1085/jgp.102.1.25

Paulais, M., and J. Teulon. 1990. cAMP-activated chloride channel in the basolateral membrane of the thick ascending limb of the mouse kidney. *J. Membr. Biol.* 113:253–260. http://dx.doi.org/10.1007/BF01870076

Picollo, A., A. Liantonio, M.P. Didonna, L. Elia, D.C. Camerino, and M. Pusch. 2004. Molecular determinants of differential pore blocking of kidney CLC-K chloride channels. *EMBO Rep.* 5:584–589. http://dx.doi.org/10.1038/sj.embor.7400169

Pusch, M. 2004. Structural insights into chloride and proton-mediated gating of CLC chloride channels. *Biochemistry.* 43:1135–1144. http://dx.doi.org/10.1021/bi0359776

Pusch, M., S.E. Jordt, V. Stein, and T.J. Jentsch. 1999. Chloride dependence of hyperpolarization-activated chloride channel gates. *J. Physiol.* 515:341–353. http://dx.doi.org/10.1111/j.1469-7793.1999.341ac.x

Rychkov, G.Y., M. Pusch, D.S. Astill, M.L. Roberts, T.J. Jentsch, and A.H. Bretag. 1996. Concentration and pH dependence of skeletal muscle chloride channel ClC-1. *J. Physiol.* 497:423–435. http://dx.doi.org/10.1113/jphysiol.1996.sp021778

Scholl, U., S. Hebeisen, A.G. Janssen, G. Müller-Newen, A. Alekov, and C. Fahlke. 2006. Barttin modulates trafficking and function of ClC-K channels. *Proc. Natl. Acad. Sci. USA.* 103:11411–11416. http://dx.doi.org/10.1073/pnas.0601631103

Sepúlveda, F.V., L. Pablo Cid, J. Teulon, and M.I. Niemeyer. 2015. Molecular aspects of structure, gating, and physiology of pH-sensitive background K2P and Kir K^+-transport channels. *Physiol. Rev.* 95:179–217. http://dx.doi.org/10.1152/physrev.00016.2014

Staruschenko, A. 2012. Regulation of transport in the connecting tubule and cortical collecting duct. *Compr. Physiol.* 2:1541–1584.

Stölting, G., M. Fischer, and C. Fahlke. 2014. CLC channel function and dysfunction in health and disease. *Front. Physiol.* 5:378.

Teulon, J., S. Lourdel, A. Nissant, M. Paulais, R. Guinamard, P. Marvao, and M. Imbert-Teboul. 2005. Exploration of the basolateral chloride channels in the renal tubule using the patch-clamp technique. *Nephron, Physiol.* 99:p64–p68. http://dx.doi.org/10.1159/000082972

Uchida, S., and S. Sasaki. 2005. Function of chloride channels in the kidney. *Annu. Rev. Physiol.* 67:759–778. http://dx.doi.org/10.1146/annurev.physiol.67.032003.153547

Waldegger, S., and T.J. Jentsch. 2000. Functional and structural analysis of ClC-K chloride channels involved in renal disease. *J. Biol. Chem.* 275:24527–24533. http://dx.doi.org/10.1074/jbc.M001987200

Waldegger, S., N. Jeck, P. Barth, M. Peters, H. Vitzthum, K. Wolf, A. Kurtz, M. Konrad, and H.W. Seyberth. 2002. Barttin increases surface expression and changes current properties of ClC-K channels. *Pflugers Arch.* 444:411–418. http://dx.doi.org/10.1007/s00424-002-0819-8

Weinstein, A.M. 2001. A mathematical model of rat cortical collecting duct: determinants of the transtubular potassium gradient. *Am. J. Physiol. Renal Physiol.* 280:F1072–F1092.

Weinstein, A.M. 2005. A mathematical model of rat distal convoluted tubule. II. Potassium secretion along the connecting segment. *Am. J. Physiol. Renal Physiol.* 289:F721–F741. http://dx.doi.org/10.1152/ajprenal.00044.2005

Wu, P., M. Wang, H. Luan, L. Li, L. Wang, W.H. Wang, and R. Gu. 2013. Angiotensin II stimulates basolateral 10-pS Cl channels in the thick ascending limb. *Hypertension.* 61:1211–1217. http://dx.doi.org/10.1161/HYPERTENSIONAHA.111.01069

Yusef, Y.R., L. Zúñiga, M. Catalán, M.I. Niemeyer, L.P. Cid, and F.V. Sepúlveda. 2006. Removal of gating in voltage-dependent ClC-2 chloride channel by point mutations affecting the pore and C-terminus CBS-2 domain. *J. Physiol.* 572:173–181. http://dx.doi.org/10.1113/jphysiol.2005.102392

Zaika, O., M. Mamenko, N. Boukelmoune, and O. Pochynyuk. 2015. IGF-1 and insulin exert opposite actions on ClC-K2 activity in the cortical collecting ducts. *Am. J. Physiol. Renal Physiol.* 308:F39–F48. http://dx.doi.org/10.1152/ajprenal.00545.2014

SUPPLEMENTAL MATERIAL

Pinelli et al., http://www.jgp.org/cgi/content/full/jgp.201611623/DC1

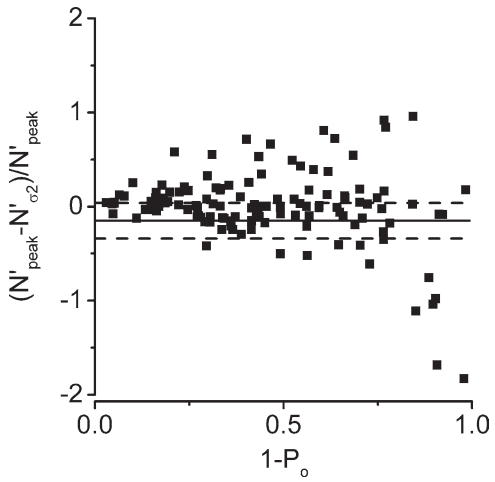

Figure S1. **Comparison of two methods for estimating the number of active channels on patches.** The number of active channels (N′) was determined in each stretch of data from (1) the peak current amplitude ($N'_{peak} = I_{peak}/i$) and (2) the variance of the patch current ($N'_{\sigma 2}$) as described in Materials and methods. The graph is a modified Bland Altman analysis where ($N'_{peak} - N'_{\sigma 2}$)/$N'_{peak}$ is plotted against $1 - P_o$ ($=\sigma^2/<I>*i$). Each point is a measurement from a stretch of recording at either V_m −80 mV or V_m 80 mV. The continuous line is the mean of 130 determinations, and 95% agreement interval limits (mean ± 1.96*SEM) are represented as dashed lines. Only recordings yielding values within the 95% agreement interval where taken as valid for the estimation of N′ and P_o.

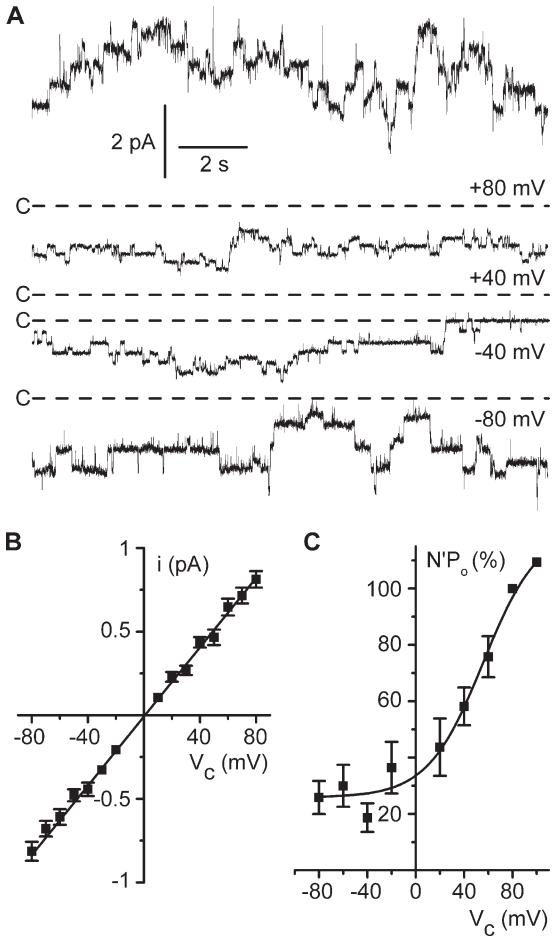

Figure S2. **Channel voltage dependence in the cell-attached configuration.** (A) Representative current recordings at the clamp membrane potentials (V_c) values indicated on the right side of each trace. CNTs were bathed in physiological saline solution, and pipettes were filled with a 5 mM Ca^{2+}–containing NMDG-Cl solution set at pH 7.4. The dashed lines (C-) indicate the closed channel current level for each clamp potential, measured after acidification of the intracellular compartment as described in Materials and methods. (B) Mean i/V_c relationship obtained in the condition given in A. Each point is the mean of 12 determinations, and SEM is shown as error bars when larger than symbols. (C) $N'P_o/V_c$ relationship obtained in the conditions given in A. $N'P_o$ values were normalized to values at V_c 80 mV on the same patch. Each point is the mean of nine measurements, except at V_c 100 mV where $n = 2$, and SEM is shown as error bars. The line is a nonlinear least squares fit of mean data points using the Boltzmann equation.

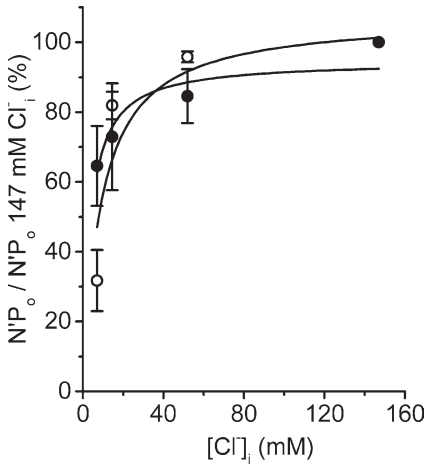

Figure S3. **Channel sensitivity to intracellular chloride concentration.** Cell-excised inside-out membrane patches were exposed to 7–147 mM internal Cl^- solutions, and currents were recorded at V_m −80 mV (●) or V_m 80 mV (○). Each $N'P_o$ value at a given internal Cl^- concentration was normalized to the paired $N'P_o$ at 147 mM Cl^- on the same patch. Data are means of measurements from three to seven patches, and SEM is shown as error bars. Lines are fits of mean data points using a rectangular hyperbola equation yielding $K_{1/2}$ values of 3.6 ± 1.3 mM internal chloride at V_m −80 mV (R^2 = 0.879) and 9 ± 5.5 mM internal chloride at V_m 80 mV (R^2 = 0.832).

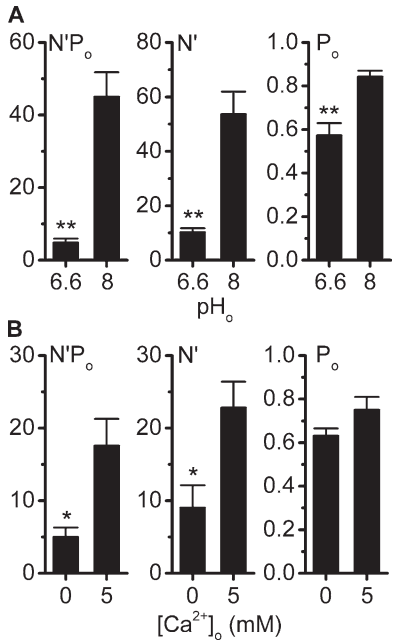

Figure S4. **pH_o and $[Ca^{2+}]_o$ also modulate the number of active channels.** Experiments were performed under symmetrical NMDG-Cl solutions, at V_m 80 mV. (A and B) $N'P_o$ was measured within 2 min after patch excision into a pH_i 7.4 and calcium-free solution under either pH_o 6.6 or 8 ($[Ca^{2+}]_o$ 5 mM; A) or external calcium-free or 5 mM Ca^{2+} conditions (pH_o 7.4; B). The number of active channels (N′) was determined by peak current measurements and validated by stationary noise analysis (see Materials and methods), and only recordings yielding ΔN′/N′ values within the 95% agreement interval were taken as valid (pH_o 6.6: *n* = 5 out of 7; pH_o 8: *n* = 6 out of 7; $[Ca^{2+}]_o$ 0: *n* = 3 out of 5; $[Ca^{2+}]_o$ 5 mM: *n* = 6 out of 6). Results are given as means, and SEM is shown as error bars. *, P < 0.01; **, P < 0.005, unpaired Student's *t* test.

Table S1. **Effects of pH_i, pH_o, and $[Ca^{2+}]_o$ on single-channel conductive properties**

Condition	g	E_{rev}
	pS	*mV*
pH_i 7.0 (7)	11.4 ± 0.3	0.1 ± 0.3
pH_i 7.4 (12)	13.0 ± 0.5	1.0 ± 0.4
pH_i 7.8 (6)	11.6 ± 0.3	0.5 ± 0.4
pH_o 6.6 (6)	12.4 ± 0.5	1.1 ± 0.4
pH_o 8.0 (9)	13.4 ± 0.1	0.4 ± 0.2
$[Ca^{2+}]_o$ 0 mM (5)	12.5 ± 0.2	0.3 ± 0.6
$[Ca^{2+}]_o$ 5 mM (5)	12.3 ± 0.5	0.5 ± 0.7

Single-channel conductances (g) and reversal potentials (E_{rev}) were determined in the conditions given in the left column. Data are given as means ± SEM for the number of observations in parentheses. Neither g nor E_{rev} were significantly affected by pH_i, pH_o, or $[Ca^{2+}]_o$ ($P > 0.2$ for each condition, unpaired *t* test).